ISSN 0021-3640, JETP Letters, 2023, Vol. 118, No. 7, pp. 502–507. © Pleiades Publishing, Inc., 2023.
ISSN 0021-3640, JETP Letters, 2023. © Pleiades Publishing, Inc., 2023.
Russian Text © The Author(s), 2023, published in Pis'ma v Zhurnal Eksperimental'noi i Teoreticheskoi Fiziki, 2023, Vol. 118, No. 7, pp. 513–518.

CONDENSED MATTER

Convolutional Neural Networks for Predicting Morphological and Nonlinear Optical Properties of Thin Films of Quasi-Two-Dimensional Materials

A. A. Popkova[a,*] (ORCID: 0000-0002-4758-6833) and A. A. Fedyanin[a] (ORCID: 0000-0003-4708-6895)

[a] *Faculty of Physics, Moscow State University, Moscow, 119991 Russia*

**e-mail: popkova@nanolab.phys.msu.ru*

Received August 10, 2023; revised August 24, 2023; accepted August 26, 2023

Two-dimensional materials are promising candidates for the creation of flat photonics devices. The main problem of using such materials for applied applications is the complexity of creating films of specified geometric parameters. The films of two-dimensional materials made by exfoliation or chemical deposition methods are usually randomly distributed over a large area and have a large thickness spread. In this paper, we use convolutional neural networks to predict the film thickness of a quasi-two-dimensional material based on optical microscopy data. Hexagonal boron nitride, which is actively used in the creation of flat electronic and optoelectronic devices, was chosen as a test material. Due to the high spatial resolution of microscopy, it is possible to achieve high accuracy in predicting the thicknesses of flat areas of the sample, which allows for rapid characterization of structures. In addition, using the example of the signal of the third optical harmonic, we show the possibility of predicting the magnitude of the nonlinear optical response of the film, which expands the scope of the method.

DOI: 10.1134/S0021364023602725

1. INTRODUCTION

Graphene, transition metal dichalcogenides and hexagonal boron nitride (hBN) are the most well-known representatives of two-dimensional materials that attract a lot of attention due to their unique electronic and optical properties [1]. Tunable band gap [2], ultrafast carrier dynamics [3, 4], bright photoluminescence [5], optical anisotropy [6] and saturated absorption [7] inherent in two-dimensional materials are promising properties for use in applied photonics and optoelectronics devices. Due to the background of the active development of graphene electronics devices [8], hBN is becoming increasingly popular. While most two-dimensional materials are metals or semiconductors, hBN is a dielectric with a band gap of about 6 eV [9], having a smooth uncharged surface, which allows it to be used as substrates and dielectric layers of composite two-dimensional devices [10]. One of the main problems in the manufacture of complex multilayer structures based on two-dimensional materials is the fabrication of films of a given thickness in the range from units to hundreds of nanometers. The fabrication of two-dimensional films is most often carried out either by chemical methods that do not provide precision control of the thickness and quality of the film, or by mechanical exfoliation, as a result of which fragments of films with different numbers of layers are randomly scattered over the surface of the receiving substrate [11]. In the latter case, the impossibility of manufacturing films of the specified parameters can be partially compensated by the accurate determination of the thicknesses of the fabricated samples. The existing methods of atomic force microscopy, Raman scattering of light and photoluminescent spectroscopy make it possible to accurately determine the thickness of films, but they are ineffective when working with large areas, since they require a lot of time to search and identify a separate structure [12]. One of the approaches in this situation is the joint application of optical microscopy and artificial neural networks (ANN), which have shown significant advantages in computer vision tasks, such as image segmentation and object classification [13, 14]. In recent years, the prospects of using ANN for the analysis of experimental data and the design of structures for the required properties of [15–18] have been shown, as well as the physical implementation of ANN based on optical structures [19, 20]. A number of articles have shown the possibility of determining the thicknesses of thin films of two-dimensional materials from measured hyperspectral images of a sample using convolutional neural networks [21, 22]. However, the measurement of hyperspectral images requires the use of sophisticated equipment, which often does not allow achieving high spatial resolution.

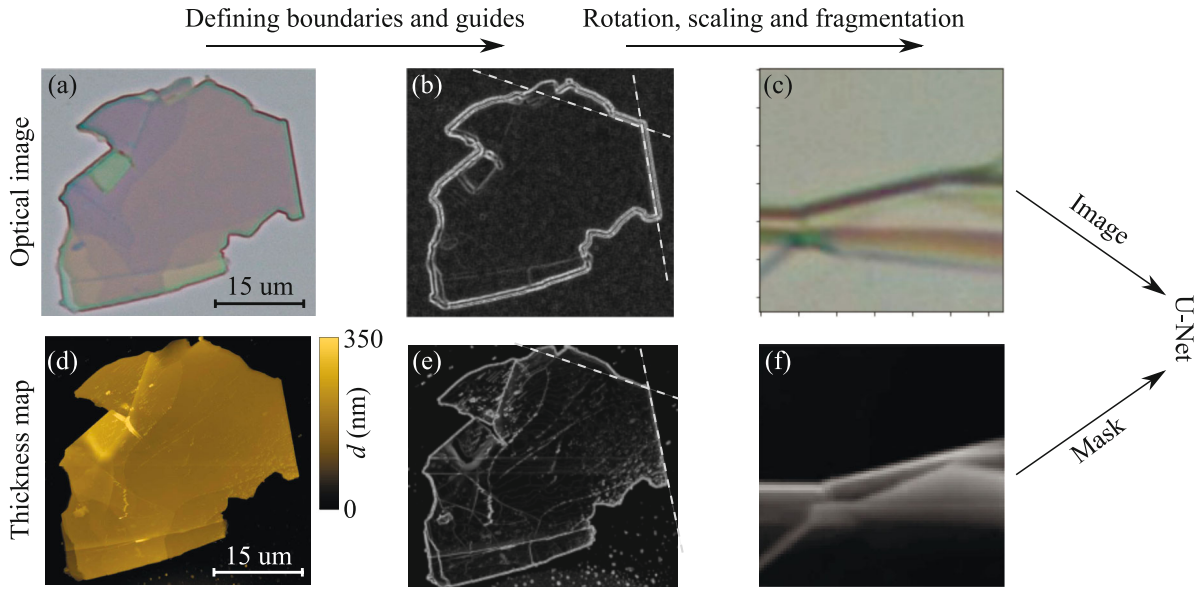

Fig. 1. (Color online) Dataset assembly scheme for training a neural network. The top row is optical images of hBN flakes: (a) original image of hBN flake, (b) map of (white lines) flake boundaries and (dotted lines) calculated guides, and (c) the dataset element obtained after fragmentation. The bottom row is thickness atomic force microscopy of (d) hBN flake, (e) (white lines) flake boundaries and (dotted lines) calculated guides, and (f) the mask obtained after fragmentation corresponding to the element (c).

In this paper, using an convolutional neural network of the U-Net architecture [23], the possibility of predicting the thicknesses of hexagonal boron nitride films from optical images of the sample is shown, which not only makes the characterization process fast and accessible, but also allows achieving high spatial resolution. An additional advantage of the method is the possibility of its use for predicting not only morphological, but also optical properties of the sample, including nonlinear optical ones, which are actively used for non-invasive characterization of nanostructures [24]. This approach is shown by the example of a signal of the third optical harmonic and demonstrates high prediction accuracy.

2. PREDICTION OF BORON NITRIDE FILM THICKNESS

The neural network was trained on optical images of fragments of thin films (flakes) of hexagonal boron nitride made by the standard method of mechanical exfoliation followed by transfer using polymethylmethacrylate (PMMA) to a fused quartz substrate. As a result of this method, hBN flakes of various thicknesses with lateral dimensions of tens of micrometers are randomly located on the substrate surface. The images of the samples were obtained using an Olympus BX53 optical microscope in a transmission and reflection illumination scheme. A color CMOS camera was used as a detector, which allows obtaining high-resolution RGB images with 8 bits depth. An example of a flake image with areas of different thicknesses is shown in Fig. 1a. It can be seen that when using white illumination, parts of the sample having different thicknesses turn out to be colored in different colors, which is due to the effect of light interference in thin films. The flake thicknesses were determined using an NT-MDT NTEGRA atomic force microscope operating in semi-contact mode. The characteristic thickness of the cantilever, which determines the accuracy of scanning, was approximately 10 nm. The thickness map of the sample corresponding to the optical image of flake is shown in Fig. 1d. The thicknesses of all the samples studied were found to lie in the range from 2 to 180 nm, with the exception of a small high flake region, shown in Fig. 1, whose thickness is about 350 nm. This area was excluded from further work, since the sample does not have other elements of such thickness, and therefore this value should be considered deviant. A histogram of the distribution of film thicknesses by structures is shown in Fig. 2. The observed distribution does not correspond to the normal one, but it covers the studied range quite fully.

As a dataset for training a neural network, an option consisting of image-mask pairs was chosen. Thickness maps were used as masks for ANN training. To compare pairs of images with each other, the boundaries of the flakes were found using the gradient method, after which the positions and rotation angles of the guide axes were determined, relative to which the scaling and rotation of the images were performed (Fig. 1b). The images of the masks were subjected to additional smoothing and alignment to compensate for defects caused by the method of measuring thick-

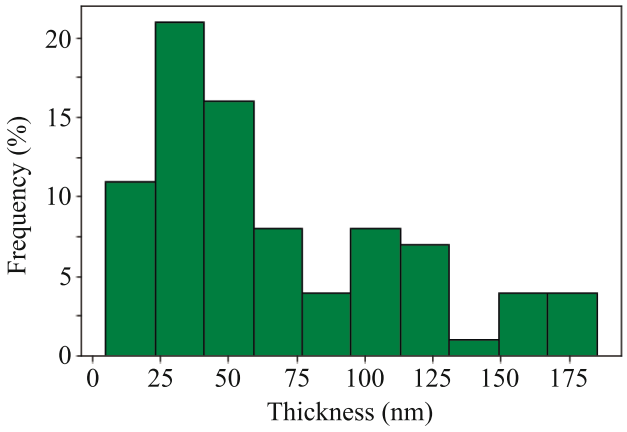

Fig. 2. (Color online) Histogram of the thickness distribution of hBN samples by dataset.

ness maps. Since the set of experimental samples is limited and amounts to about 80 pieces, an extension of the dataset is required to train the ANN. For this, a method of fragmentation using a square grid was chosen, in which the number of dataset elements is increased by splitting the available images into smaller parts with the possibility of applying additional augmentation to them (random rotation or random deformation) (Fig. 1c). To select only the target images, a binary mask classifier based on the average pixel value on the mask was used, determined the presence of a flake on it. Images with an average value of less than 1 nm, that is, containing only a substrate, were discarded. The size of the dataset element was selected for optimal network speed and amounted to 128 pixels to predict the thickness of the sample and 32 pixels to predict the nonlinear optical response. The result size of the dataset for predicting the thickness of the sample was about 10^4 elements. Since the intensity of an 8-bit RGB image lies in the range from 0 to 255, for the convenience of learning, the images were scaled using min-max normalization so that the target signal range lies in the range from 0 to 1. The final dataset was divided into train, test, and validation in a proportion of 70:20:10.

Table 1. Quality of predictions Q (in percent) of the thickness of the hBN sample for its various configurations on the full dataset and dataset that does not contain elements with significant kinks

Number of layers/kernel size	Full dataset	Dataset without kinks
10/(1 × 1)	65	91
10/(3 × 3)	68	92
16/(1 × 1)	85	94
16/(3 × 3)	83	95
16/(5 × 5)	88	95

To predict the film thicknesses, a convolutional ANN of the U-Net type [22] was built, trained and tested, solving the problem of pixel-by-pixel prediction of the sample mask. The variable network parameters were the number of network layers, the size of the used convolution kernel, and the amount of data supplied to the input (batch size). The ANN was modeled in the Python software environment using the PyTorch, Numpy, and MatPlotLib packages. The pixel-by-pixel mean standard deviation (MSE) of the thickness values of the predicted map from the target mask was used as a loss function. To assess the accuracy of the prediction, the average fraction of pixels in the batch images was used, for which the thickness deviation between the predicted and the set one was no more than 2 nm:

$$Q = \frac{1}{N}\sum i\Big|_{|d_t - d_{\mathrm{pr}}|<2}, \qquad (1)$$

where N is the total number of pixels in the image, d_t and d_{pr} are the target and predicted pixel thickness values, respectively. The deviation value of 2 nm was taken as the maximum value of thickness fluctuations obtained when determining the thickness of the mask by atomic force microscopy. To assess the network's ability to generalize an independent data set, a cross-validation approach was used, alternately excluding one of the subsamples. A typical view of the learning curve of the network, as well as the dependence of the prediction accuracy on the epoch number (iteration of training on a full dataset) for an ANN with ten layers using convolution kernels of size 3 × 3, are shown in Fig. 3a. The monotonically decreasing curve of the loss function, gradually entering saturation, and the corresponding curve of increasing the accuracy of thickness prediction indicates a good ability to train the model. The maximum achieved values of the prediction accuracy of networks of various configurations are shown in Table 1. The highest prediction accuracy of 88% was achieved for an ANN consisting of 16 layers and using convolution kernels of size 5 × 5. A typical view of the target and predicted thickness map for this case is shown in Fig. 3b. Analysis of the type of thickness maps allows us to conclude that the greatest contribution to the loss function is made by dataset elements with significant kinks. The exception from the dataset of elements containing thickness differences of more than 15 nm allowed to increase the accuracy of the ANN predictions to 95%. A comparison of the accuracy obtained on the full dataset and a dataset that does not contain kinks demonstrates an increase in the accuracy of predictions for all configurations of the ANN, which confirms the influence of the quality of the dataset images. Special attention should be paid to the fact that for an optimal dataset, network configurations consisting of layers with con-

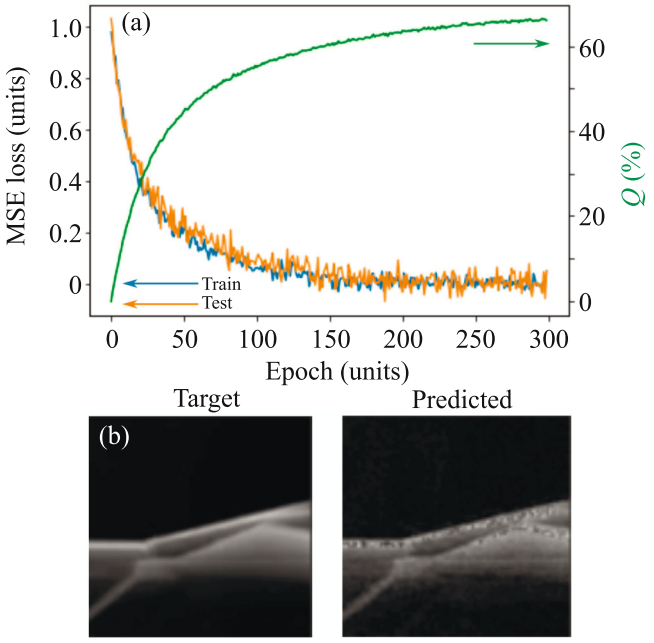

Fig. 3. (Color online) (a) Loss function for the (blue line) train and (orange line) test sets and (green line) the prediction quality versus the epoch number. (b) Image of the target mask for (left) the dataset element and (right) the result of the corresponding prediction of the ANN.

volution kernels of 1 × 1 are quite effective, which demonstrates the possibility of simplifying the used architecture.

3. PREDICTION OF NONLINEAR OPTICAL SIGNAL FROM BORON NITRIDE FILMS

The second part of the work was the prediction of the nonlinear optical (NLO) response of hBN films from optical images. The signal of the third optical harmonic generated by the sample was chosen. In this case, the distribution maps of the third optical harmonic power over the sample surface were used as masks, obtained by scanning flakes with a focused beam of a femtosecond titanium-sapphire laser [25]. The focal length was 2 microns, the sample offset step, which determines the resolution of the final image, was 0.3 microns. To assemble the dataset, the resolution of the maps was increased by taking a weighted average from the elements, and the resolution of optical images was lowered by taking the average from neighboring pixels (AveragePool). As a result, a dataset consisting of "image–mask" pairs with a spatial element size of 32 pixels was assembled. An example of a dataset mask is shown in Fig. 4a. It can be seen that there are kinks on the element, the nonlinear response from which significantly exceeds the average value of the sample. This effect is caused by the occurrence of stress leading to deformation of the crystal lattice of the material and a local increase in the efficiency of nonlinear optical effects [26].

On this dataset, the training of ANN similar to those used to predict the thickness of samples was carried out. As a measure of prediction accuracy, the proportion of pixels for which the target and predicted capacities differ by no more than 0.5 pW was used. The obtained prediction accuracy is shown in Table 2 (column "NLO") and turns out to be lower than similar values for the thickness prediction task. To analyze the results, the dependences of the third harmonic power distribution on the pixel number in the slice of the dataset element were constructed. For a dataset element with the thickness difference of 25 nm (Fig. 4b), the main error in predicting the nonlinear response is observed in the area of the height difference. The error in predicting the signal from a flat section of the sample is negligible. For an element having a stepped structure with a monotonous change in thickness (Fig. 4c), the accuracy of predicting the response turns out to be higher, due to the absence of elements in the dataset that introduce a significant error.

It is worth noting that the obtained accuracy can probably be increased by further optimization of the parameters of the used ANN, however, even the cur-

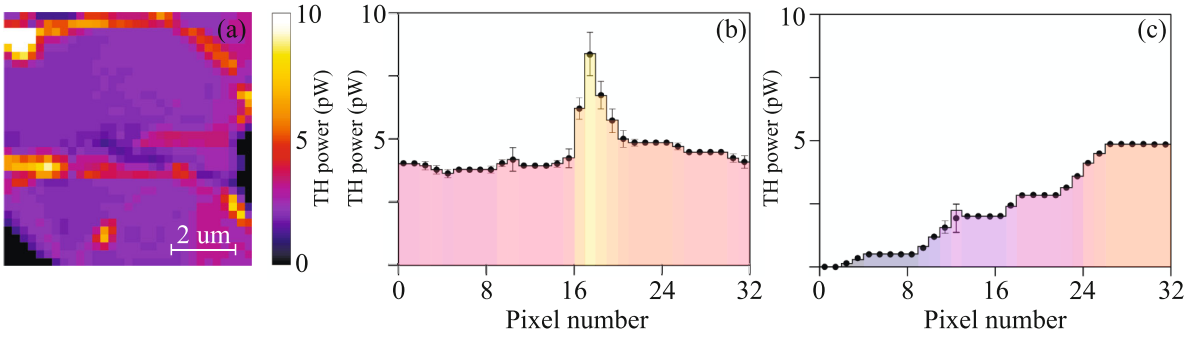

Fig. 4. (Color online) (a) Dataset element for predicting the magnitude of the third harmonic signal (non-normalized). (b, c) Third harmonic power versus the pixel number for the slice of two dataset elements (b) with and (c) without significant kinks. The lines show experimental data, the circles with error bars show the network predictions averaged over ten attempts.

Table 2. Quality of predictions Q (in percent) of the ANN for the determining the thickness (column "thickness") and the nonlinear response (column "NLO") of the sample

Number of layers/kernel size	Thickness	NLO
10/(1 × 1)	65	56
10/(3 × 3)	68	64
16/(1 × 1)	85	72
16/(3 × 3)	83	75
16/(5 × 5)	88	78

rently available values have sufficient predictive ability for practical applications.

4. CONCLUSIONS

To conclude, the possibility of predicting morphological and nonlinear optical properties of thin films of hexagonal boron nitride using convolutional neural networks of the U-Net architecture is shown. The maximum achieved accuracy of predicting the thickness of the sample for the experimental dataset was 88%. It is shown that the obtained value can be improved up to 95% by purification the dataset from elements containing a significant difference in thickness, which are also irrelevant for practical applications. In addition, the possibility of predicting the nonlinear optical response of a sample, in particular the third optical harmonic intensity, with an accuracy of up to 78%, is demonstrated. The lower accuracy of predicting the intensity of the third optical harmonic compared to the thickness is due to the smaller size of the dataset, as well as the existing ambiguity in the dependence of the nonlinear response signal on the thickness of the sample [25].

The obtained results show the prospects of using convolutional neural networks for rapid optical and nonlinear optical characterization of samples of quasi-two-dimensional materials, which is necessary both for fundamental point of view and for the practical use of such structures in the fabrication of more complex electronics and optoelectronics devices. The code of the work and examples of the dataset used are available at the link https://github.com/AnyaPopkova/JETP_2D.git.

ACKNOWLEDGMENTS

We are grateful to I.M. Antropov and V.O. Bessonov for help in carrying out measurements and useful discussions.

FUNDING

The work was supported of the Foundation for the Development of Science and Education Intellect and the Foundation for the Advancement of Theoretical Physics and Mathematics BASIS (project no. 19-2-6-28-1).

CONFLICT OF INTEREST

The authors declare that they have no conflicts of interest.

REFERENCES

1. F. Xia, H. Wang, D. Xiao, M. Dubey, and A. Ramasubramaniam, Nat. Photon. **8**, 899 (2014).
2. S. Susarla, A. Kutana, J. A. Hachtel, V. Kochat, A. Apte, R. Vajtai, J. C. Idrobo, B. I. Yakobson, C. S. Tiwary, and P. M. Ajayan, Adv. Mater. **29**, 1702457 (2017).
3. J. M. Dawlaty, S. Shivaraman, M. Chandrashekhar, F. Rana, and M. G. Spencer, Appl. Phys. Lett. **92**, 042116 (2008).
4. A. A. Popkova, A. A. Chezhegov, M. G. Rybin, I. V. Soboleva, E. D. Obraztsova, V. O. Bessonov, and A. A. Fedyanin, Adv. Opt. Mater. **10**, 2101937 (2022).
5. Y. Chen, J. Xi, D. O. Dumcenco, Z. Liu, K. Suenaga, D. Wang, Z. Shuai, Y.-S. Huang, and L. Xie, ACS Nano **7**, 4610 (2013).
6. L. V. Kotova, L. A. Altynbaev, M. O. Zhukova, B. T. Hogan, A. Baldycheva, M. A. Kaliteevski, and V. P. Kochereshko, Bull. Russ. Acad. Sci.: Phys. **86**, 813 (2022).
7. C. Ma, C. Wang, B. Gao, J. Adams, G. Wu, and H. Zhang, Appl. Phys. Rev. **6**, 041304 (2019).
8. Y. Wu, D. B. Farmer, F. Xia, and P. Avouris, Proc. IEEE **101**, 1620 (2013).
9. G. Cassabois, P. Valvin, and B. Gil, Nat. Photon. **10**, 262 (2016).
10. E. N. Oparin, M. O. Zhukova, V. G. Bulgakova, S. A. Pozdnyakova, and A. N. Tcypkin, Photon. Russ. **14**, 264 (2020).
11. R. Frisenda, E. Navarro-Moratalla, P. Gant, D. P. De Lara, P. Jarillo-Herrero, R. V. Gorbachev, and A. Castellanos-Gomez, Chem. Soc. Rev. **47**, 53 (2018).
12. A. Crovetto, P. R. Whelan, R. Wang, M. Galbiati, S. Hofmann, and L. Camilli, ACS Appl. Mater. Interfaces **10**, 25804 (2018).
13. E. Moen, D. Bannon, T. Kudo, W. Graf, M. Covert, and D. van Valen, Nat. Methods **16**, 1233 (2019).
14. A. Garcia-Garcia, S. Orts-Escolano, S. Oprea, V. Villena-Martinez, P. Martinez-Gonzalez, and J. A. Garcia-Rodriguez, Appl. Soft Comput. **70**, 41 (2018).
15. K. R. Safronov, V. O. Bessonov, and A. A. Fedyanin, JETP Lett. **114**, 360 (2021).
16. X. Han, Z. Fan, Z. Liu, C. Li, and L. J. Guo, InfoMat **3**, 432 (2021).
17. S. An, C. Fowler, B. Zheng, M. Y. Shalaginov, H. Tang, H. Li, L. Zhou, J. Ding, A. M. Agarwal, C. Rivero-Baleine, K. A. Richardson, T. Gu, J. Hu, and H. Zhang, ACS Photon. **6**, 3196 (2019).
18. R. S. Minyazev, A. A. Rumyantsev, S. A. Dyganov, and A. A. Baev, Bull. Russ. Acad. Sci.: Phys. **82**, 1685 (2018).

19. A. I. Musorin, A. S. Shorokhov, A. A. Chezhegov, T. G. Baluyan, K. R. Safronov, A. V. Chetvertukhin, A. A. Grunin, and A. A. Fedyanin, Phys. Usp. **66** (9) (2023). https://doi.org/10.3367/UFNr.2023.07.039505
20. T. Yan, J. Wu, T. Zhou, H. Xie, F. Xu, J. Fan, L. Fang, X. Lin, and Q. Dai, Phys. Rev. Lett. **123**, 023901 (2019).
21. Y. Saito, K. Shin, K. Terayama, S. Desai, and M. Onga, Y. Nakagawa, Y. M. Itahashi, Y. Iwasa, M. Yamada, and K. Tsuda, npj Comput. Mater. **5**, 1 (2019).
22. X. Dong, H. Li, Z. Jiang, T. Grünleitner, I. Güler, J. Dong, and A. W. Koch, ACS Nano **15**, 3139 (2021).
23. O. Ronneberger, P. Fischer, and T. Brox, in *Medical Image Computing and Computer-Assisted Intervention MICCAI 2015, Proceedings of the 18th International Conference, Münich, Germany* (Springer Int., 2015), Part III 18, p. 234.
24. M. Yu. Eremchev, JETP Lett. **118,** 288 (2023).
25. A. A. Popkova, I. M. Antropov, J. E. Froch, S. Kim, I. Aharonovich, V. O. Bessonov, A. S. Solntsev, and A. A. Fedyanin, ACS Photon. **8**, 824 (2021).
26. X. S. Kong, X. Y. Wu, L. Geng, and W. D. Yu, Front. Phys. **10**, 1032671 (2022).